Full Paper

Synthesis of Gem-Dichlorocyclopropane Allylcarveol and Their Effect in Protecting Against Corrosion of Mild Steel in 1.0 M HCl

Samira Khachouf,[1,*] and Abdeslam Ansari[2]

[1]*Research team of Chemistry of Bioactive Molecules and the Environment, Faculty of Science, Moulay Ismail University, BP 11201 Zitoune, Meknès, Morocco*

[2]*Laboratory of Natural Substances & Synthesis and Molecular Dynamics, Faculty of Sciences and Techniques, Moulay Ismail University of Meknes, BP 509, 52000, Errachidia, Morocco*

*Corresponding Author, Tel.: +212 668651142

E-Mail: samirakharhouf@yahoo.fr

Abstract- In this work, the gem-dichlorocyclopropane allylcarveols **Carb_8-Carb_10** namely: *1-allyl-5-(2,2-dichloro-1-methylcyclopropyl-2-methylcyclohex-2-en-1-ol*, *1-(but-3-en-2-yl)-5-(2,2-dichloro-1-methylcyclopropyl)-2-methylcyclohex-2-en-1-ol* and *5-(2,2dichloro-1-methyl cyclopropyl)-1-((2,2-dichloro-1-methylcyclopropyl)methyl)-2 methylcyclohex-2-en-1-ol* were synthesized from R-(-)-Carvone (the major constituent of spearmint oil) derivatives. In this synthesis, we used the technique of liquid-liquid phase transfer catalysis. These compounds were evaluated as corrosion inhibitors of steel in 1 M HCl by gravimetric methods. The acquired results prove that the inhibitory efficiency increases with concentration. The temperature effect on the corrosion behavior of steel in 1 M HCl in the presence and absence of inhibitors at 1×10^{-2} mol/l was studied in the temperature range of 313–343 K, the activation parameters of the corrosion reaction were calculated using the Arrhenius equation, and the transition state equation. The adsorption of this compound on Mild Steel surface obeys Freundlich's adsorption isotherm. In the theoretical computations, we used the Density Functional Theory (DFT) and Monte Carlo simulations to find the best spatial configuration of inhibitors on the steel surface.

Keywords- Synthesis; Carvone derivatives; Corrosion inhibition; Steel; Adsorption

1. INTRODUCTION

The literature review of works in the field of protection against corrosion of iron in acid medium leads to the conclusion that the inhibitory effect of these substances depends of the functional group, electrons, and length of the carbon chain of the main constituents of these substances. Indeed, researchers have thought to synthesize derivatives of natural substances based on the characteristics of final products obtained to improve their effectiveness in inhibiting corrosion. It was shown that nitrogen-containing compounds are more effective in hydrochloric acid [1]. However, sulfur-containing compounds are preferable for sulfuric acid [2,3].

In the last decade, many studies have focused on the inhibition of corrosion by the natural extracts. These were used in place of the synthetic organic inhibitors which are in most cases toxic substances. It used to be proven that Pennyroyal oil [4], Lavender oil [5], and Salvia Aucheri Mesatlantica oil [6] are excellent inhibitors for the corrosion of metal in an acid medium. Menthol [7], pulegone [8,9] and carvone [10] derivatives have already been suggested as highly effective corrosion inhibitors for steel in acid medium.

The purpose of this work is to synthesize **Carb_8** and **Carb_10** dichlorocyclopropane allylcarveols derived from Carvone derivatives; investigate their effect on the corrosion of steel in acid media by gravimetric method; examine the effect of temperature, and simulate the adsorption behavior of inhibitors to the iron surface (110). These are realized by using density functional theory (DFT) and Monte Carlo Simulation (MC).

2. MATERIALS AND METHODS

2.1. Synthesis procedure of gem-dichlorocyclopropane allylcarveols.

We mixed 2.6 mmol of allylcarveol (in 2 ml of $CHCl_3$) with 2 ml of aqueous solution NaOH 50% and a catalytic amount of triethyl benzyl ammonium chloride (TBA-Cl). After 2 hours, the mixture was introduced into 5 ml of water and extracted with ether. The organic phase was dried with $MgSO_4$, the solvent was removed with a rotary evaporator and the crude product was chromatographed on silica gel or recrystallized from petroleum ether.

Infrared (IR) spectra were recorded on Shimadzu IR-470. ^{1}H NMR spectra were figured out on a Brüker AC250 (300 MHz) spectrometer with Me_4Si as the internal standard. ^{13}C NMR spectra of $CDCl_3$ solution were recorded on Brüker AC250 (60 MHz).

2.2. Gravimetric measurements

2.2.1. Materials preparation

The corrosive solution (1M HCl) was prepared by dilution of analytical grade 37% HCl with double-distilled water. Preceding all measures, the steel specimens (0.09% P; 0.38% Si; 0.01% Al; 0.05% Mn; 0.21% C; 0.05% S and the rest iron) were smooth with sandpaper up to

1200 grade, cautiously washed with double-distilled water, skimmed by utilizing AR class ethanol, acetone and dehydrated at ambient temperature.

2.2.2. Concentration Effect

Weight measurements were made in a double-walled glass cell outfitted with a thermostat-cooling condenser. The solution volume was 100 ml, and the metal samples used had a rectangular shape (2.5 cm×2 cm×0.05 cm). The immersion time for the weight loss was 1 hour at 333 K. After the corrosion test, the specimens of steel were cautiously washed in double-distilled water, dried, and then weighed. The rinse removed loose segments of the film of the corroded samples. Duplicate experiments were carried out in every case and the mean value of the weight loss is reported. Weight loss allowed us to calculate the mean corrosion rate as expressed in mg cm^{-2} h^{-1}.

The corrosion rate (W) and inhibition efficiency E_w(%) were determined according to Eq. (1) and (2) respectively:

$$W = \frac{\Delta m}{St} \tag{1}$$

$$E_W (\%) = \frac{W_{corr} - W_{corr(inh)}}{W_{corr}} \times 100 \tag{2}$$

where:

- Δm (mg) is the difference in weight of the specimen before and after immersion in the corrosive solution

- W_{corr} is the value of corrosion weight losses of mild steel in uninhibited solutions and $W_{corr(inh)}$ is its value in inhibited solutions

- S is the area of the mild steel specimen (cm^2) and t is the exposure time (h).

2.2.3. Temperature Effect

The impact of temperature on the inhibited acid–metal reaction is very complex, due to the fact many modifications show up on the metal surface such as fast etching, desorption of inhibitor and the inhibitor itself can also endure decomposition [11]. The exchange of the corrosion rate with the temperature was once studied in 1M HCl for the duration of 1 h of immersion, each in the absence and presence of inhibitors at a concentration corresponding to the most inhibition efficiency. For this purpose, gravimetric experiments were carried out at different temperatures (313–333 K). To calculate activation thermodynamic parameters of the corrosion process, Arrhenius Eq. (3) and transition state Eq. (4) were used [12]:

$$W = A\, e^{\left(-\frac{E°a}{RT}\right)} \tag{3}$$

$$W = \frac{RT}{Nh}\, e^{\left(\frac{\Delta S°a}{R}\right)} e^{\left(-\frac{\Delta H°a}{RT}\right)} \tag{4}$$

where: E°_a means the apparent activation corrosion energy, R the universal gas constant, A is the Arrhenius preexponential factor, h is the Plank's constant, N is the Avogadro's number, ΔS°_a is the entropy of activation and ΔH°_a is the enthalpy of activation.

2.2.4. Adsorption isotherm

The information about the properties of the tested compounds is provided by the type of adsorption isotherm. To obtain the latter it is necessary to calculate the degree of surface coverage (θ) of the inhibitors by using different adsorption isotherms such as Langmuir, Frumkin and Temkin.

The Langmuir isotherm (C/θ *vs.* C) assumes that there is no interaction between the molecules adsorbed on the surface.For the Frumkin isotherm (θ *vs.* C) it assumes that there is some interaction between the adsorbents. While Temkin's (θ *vs.* lgC) represents the effect of multiple layer coverage [13].

In our study, the degree of surface coverage (θ) for different inhibitor concentrations in acidic medium was evaluated from weight loss measurements.

2.3. Theoretical examination

2.3.1. Quantum chemistry simulation

By using a Gaussian 09W software package, the density-functional [DFT] calculations were done in investigated Carvone's derivatives carb8, carb9, and carb10 in the gas phase. Entire molecules were geometrically perfected by using a DFT/B3LYP method that is associated with 6-31G++(d,p) basis sets, commonly used in the investigation of organic corrosion inhibitors [14]. Process optimization was confirmed by the absence of imaginary vibration frequencies. Next, various related molecular electronic structural parameters, including the highest occupied E_{HOMO} and lowest unoccupied E_{LUMO} molecular orbital energy as well as gap energy (ΔE_{gap}, Eq. (5)), the electronegativity (χ, Eq. (6)), the hardness (η, Eq. (7)) and the fraction of electron transfer (ΔN Eq. (8)) were calculated [15]. Also, electrostatic potential plots and frontier molecular orbitals (i.e., HOMO and LUMO) of every Carvone's derivative were calculated and figured [16].

$$\Delta E_{gap} = E_{LUMO} - E_{HOMO} \qquad (5)$$

$$\chi = \frac{E_{LUMO} - E_{HOMO}}{2} \qquad (6)$$

$$\eta = \frac{E_{HOMO} - E_{LUMO}}{2} \qquad (7)$$

$$\Delta N = \frac{\emptyset - \chi_{inh}}{2(\eta_{Fe} + \eta_{inh})} \qquad (8)$$

where $\emptyset$ has a value of 4.82 and symbolizes the size of the work function; $\eta_{Fe} = 0$ eV/mol is equal to the hardness of Fe; χ_{inh}, as well as η_{inh}, are in this order the electronegativity and the hardness of the inhibitor [17].

The Monte Carlo adsorption of the three compounds on the Fe (110) surface was studied in the real environment by the mean of the adsorption locator given in the Material studio tool [18]. The simulation was run in the box with the following size ($24.78 \times 24.78 \times 42.15$ A3), created using a vacuum slab of 26 A thicknesses. The COMPASS force field was applied to perfect all the structures of the system in the simulation procedure. The energy of adsorption (E_{ads}) of the three compounds was calculated when the system constitutes inhibitor/400 H_2O, $20 H_3O^+$, $20 Cl^-$/Fe (110) reaches the equilibrium state. This was done by submitting the resulting data to Eq. (9):

$$E_{ads} = E_{total} + E_{solution} - (E_{surface+solution} + E_{inhibitor+solution}) \qquad (9)$$

where E_{total}, $E_{surface+solution}$, $E_{inhibitor+solution}$, and $E_{solution}$ correspond respectively to the total energies of the Fe (110) surface with adsorbed inhibitor and solution, the total energy of the surface and solution, the total energy of the system except the iron crystal, and the total energy of the solution.

3. RESULTS AND DISCUSSION

3.1. Inhibitors synthesis

In the last work [19], we reported that the addition of allyl Grignard compounds **2-4** on carvone **1** leads to allylcarveols **5-7** respectively as illustrated in Scheme 1.

The dihalocyclopropanation of allylcaleols 5-7 is readily accomplished under phase transfer catalysis conditions (liquid-liquid) using chloroform, aqueous sodium hydroxide 50%, and benzyl triethylammonium chloride to obtain the corresponding bi- or tetra-halo adducts depending on the structure of the initial alcohols.

Thus, the treatment of allylcarveols **5** and **6** with dihalocarbenes in these conditions produces gem-dihalocyclopropane allylcarveols **Carb_8** and **Carb_9** respectively in good yields. However, a similar treatment with allylcarveol **7** leads to corresponding tetrachloro product **Carb_10**.
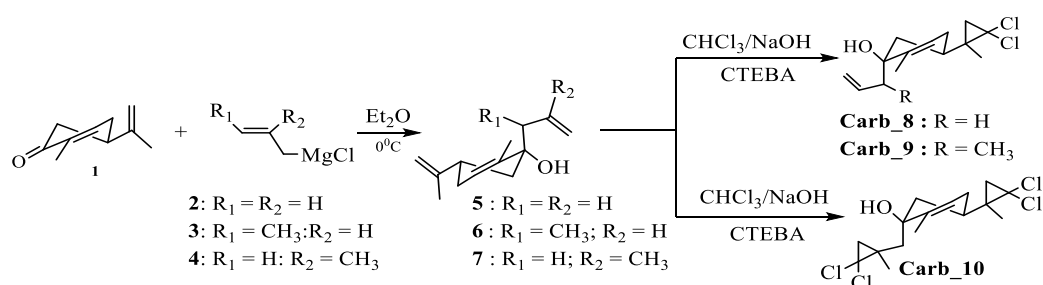
Scheme 1. Synthesis procedure of compounds **Carb_8** and **Carb_10**

The reaction is regioselective for allylcarveols **5** and **6**, but not for **7**. This regioselectivity of dihalocarbenes on the double bond of isopropyl group of allylcarveols **5** and **6** is determined by a combination of IR, ^{1}H NMR, and ^{13}C NMR analysis of corresponding gem-dihalocyclopropane allylcarveols **Carb_8** and **Carb_9** respectively (Table 1). The infrared spectra contain a narrow band, which confirms the presence of the vinyl protons of the allylic fragments (C=CH$_2$) and another band attributed to the double bond C=C. The ^{1}H NMR spectrum of both compounds **Carb_8** and **Carb_9** confirms the cyclopropanation of the double bond of the isopropyl group.

Table 1. Spectral Characterization Data of gem-dichlorocyclopropane allylcarveols **Carb_8** and **Carb_10**

| Compound	Carb_8 $C_{14}H_{14}Cl_2O$	Carb_9 $C_{15}H_{16}Cl_2O$	Carb_10 $C_{16}H_{14}Cl_4O$
Yield	76%	76%	70%
IR data	3470,3080,1635;1031, 757 cm^{-1}.	3585,3075,1635, 757 cm^{-1}	3585,3075,1635,757 cm^{-1}
^{1}H NMR data	1.26(3H,s),1.75(3H,s) 2.60 (2H, m), 5.48 (1H,s), 5.19 (1H, m), 6.0 (2H, m).	0.95(3H,d,J= 6.5 Hz),1.17 (3H, s) 2.56 (2H, m), 5.60 (1H,s),5.22(1H,m),6.0 (2H, m).	1.26(3H, s), 1.17 (2H, s), 4.76 (1H, s).
^{13}C NMR data	17.1(q), 20.5(q), 22.2 (q), 28.2(d), 29.6 (d), 32.8(d), 41.9(d), 43.0 (d), 39.6 (s), 74.9 (s), 68.4(s),67.5(s), 126.9 (d), 144.6 (s).	17.1(q), 15.2(q), 12.4 (q), 27.9 (q), 32.9 (t), 40.2(t), 44.0 (d), 37.5 (d), 37.6 (s), 67.8 (s), 75.4(s),114.7(d), 137.3(d),140.5(d), 125.2 (d).	17.1(q),20.5 (q), 22.2 (q),28.2(d), 29.6 (d), 32.8(d),41.9 (d), 43.0 (d), 39.6 (s), 74.9 (s), 68.4(s),67.5(s), 126.9 (d), 144.6 (s).

Indeed, these spectra show the absence of the massive assigned to ethylenic protons of this double bond. We also noted the existence of massif attributed to an ethylenic proton, the methyl bound to the endocyclic double bond, and the protons of the homoallylic double bond of first alcohols. While in the infrared adsorption of compound **Carb_10**, we noted the disappearance of the vibrational band corresponding to the protons of two methylenes (C=CH$_2$) and the presence of vibrational band C=C. The ^{13}C NMR of each product **Carb_8**, **Carb_9,** and **Carb_10** show that the signals of both unsaturated carbons of the endocyclic double bond stayed unchanged.

In the case of compounds **5** and **6,** their ^{13}C NMR spectrum shows that the double bond of the isopropyl group is attacked. This result is unexpected because the double bond of the isopropyl group is less substituted than the endocyclic double bond. It is notable that the electrophilic dihalocarbene is highly discriminated in favor of more alkylated olefins. This behavior of the two olefins toward dichlorocarbene is due to steric hindrance. Hence, for the allylcarveols 7, which has a substituted allylic double bond, the bis addition has been favored.

3.2. Gravimetric results
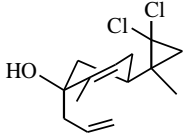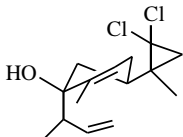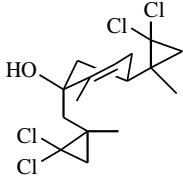
3.2.1. Inhibitor concentration effect

The values of the corrosion rate (W) and the percentage of inhibition efficiency E_w (%) got from the gravimetric methods at various concentrations of the studied compounds are shown in Table 2 and Figure 1.
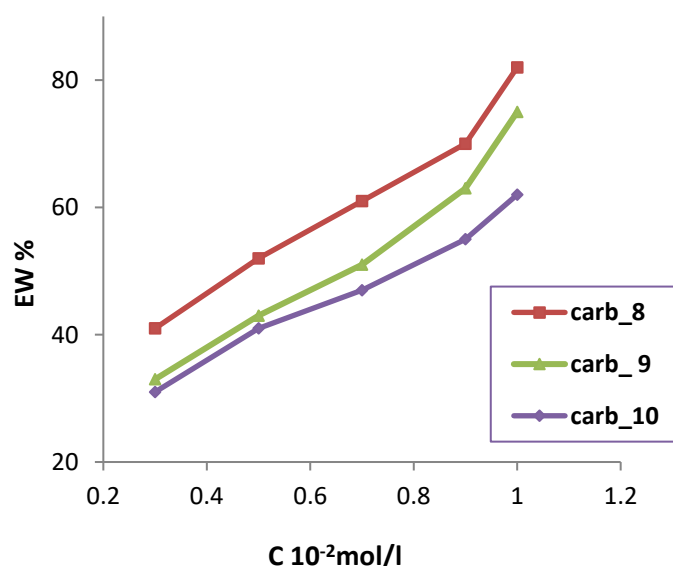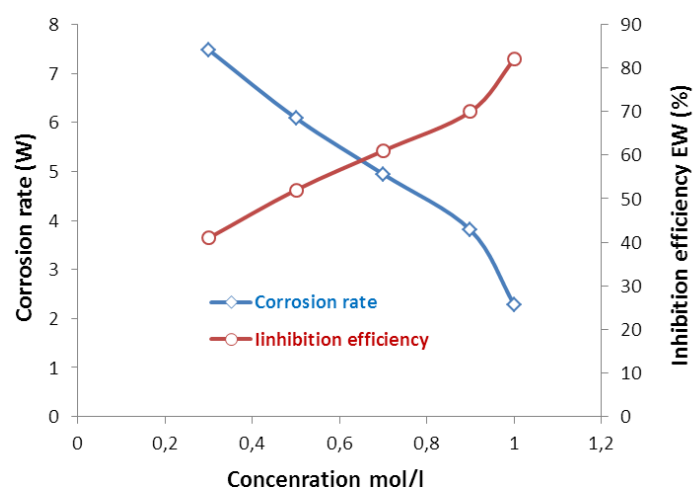

Figure 1. Variation of inhibition efficiency E_w(%) with the concentration of inhibitors **Carb_8** and **Carb_10**

The results presented in Table 2 and Figures 1 and 2 show that the inhibition efficiency E_w increases with increasing inhibitor concentration and reaches a maximum value (82%) at 1mol/L. which indicates that the three compounds **Carb_8** and **Carb_10** act as a good inhibitor for steel in molar HCl. This behavior could be caused by the blockage of the reaction sites resulting from the adsorption of the compounds on the mild steel surface and consequently its protection against the attack of active ions in the acid medium. This adsorption depends on the type of aggressive electrolyte, the surface charge, the nature of the metal, and the inhibitors chemical structure [20].

Table 2. Weight loss data for mild steel in 1 M HCl without and with different concentrations of the compounds **Carb_8** and **Carb_10** at 333K for 1h

Compounds	C 10^{-2} (mol/l)	W (mg/cm^{2}h)	E$_w$ %
	0	12.677	-
	0.3	7.479	41
	0.5	6.085	53
	0.7	4.944	61
	0.9	3.803	70
Carb_8	1	2.281	**82**
	0.3	8.506	33
	0.5	7.213	43
	0.7	6.173	51
	0.9	4.685	63
Carb_9	1	3.131	**75**
	0.3	8.772	31
	0.5	7.378	42
	0.7	6.719	47
	0.9	5.666	55
Carb_10	1	4.779	**62**

However, the corrosion rate decreased continuously with increasing the inhibitor concentration, ie, the corrosion of steel is slowed down by the gem-dichlorocyclopropane allylcarveols **Carb_8** and **carb_10**.
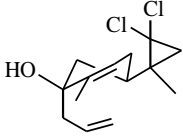

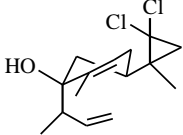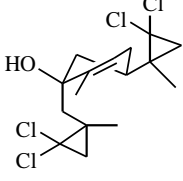**Figure 2.** Variation of the corrosion rate of steel and the inhibition efficiency against the compound Carb_8 concentration
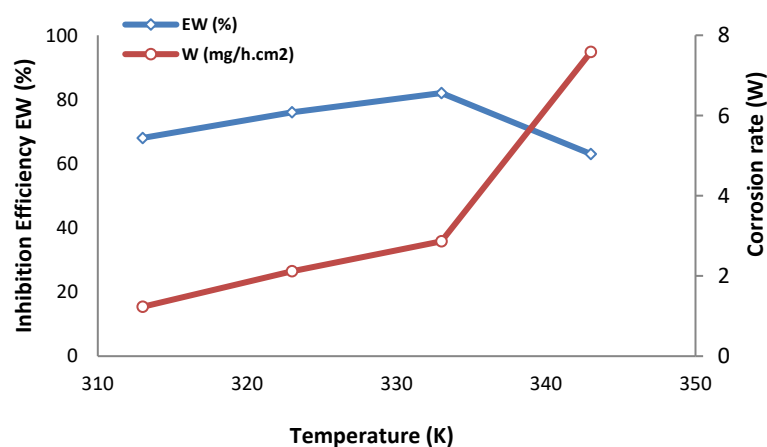
3.3. Temperature effect

The temperature effect on the behavior of steel corrosion in molar HCl with and without inhibitors is studied in the temperature range 303-343 K for 1 h of immersion at a maximal concentration (1×10^{-2} mol/l) using gravimetric measurements. The results are summarized in Table 3 and Figure 3.

Table 3. Inhibition efficiencies and weight loss data obtained with compounds **Carb_8** and **carb_10** at different temperatures at 1 h

Compounds	T (K)	W_{corr} (mg/cm²h)	W_o (mg/cm²h)	E_w %
Carb_8	313	1.231	4.478	68
	323	2.118	7.418	76
	333	2.863	12.677	**82**
	343	7.583	19.369	63
Carb_9	313	1.419	4.478	59
	323	2.367	7.418	68
	333	3.131	12.677	**75**
	343	9.014	19.369	53
Carb_10	313	1.805	4.478	48
	323	3.279	7.418	55
	333	4.779	12.677	**62**
	343	11.052	19.369	43

Figure 3. Variation of corrosion rate and inhibition efficiency as a function of temperature in the presence of compounds **Carb_8**

The examination of these results revealed that the inhibition efficiency increases with increasing temperature. It is also noted that inhibitory efficiency decreases when the temperature exceeds 333K to about 20%. This may be due to the decrease of the adsorption strength and the decrease of the inhibiting effect of the inhibitors at a temperature above 333K.
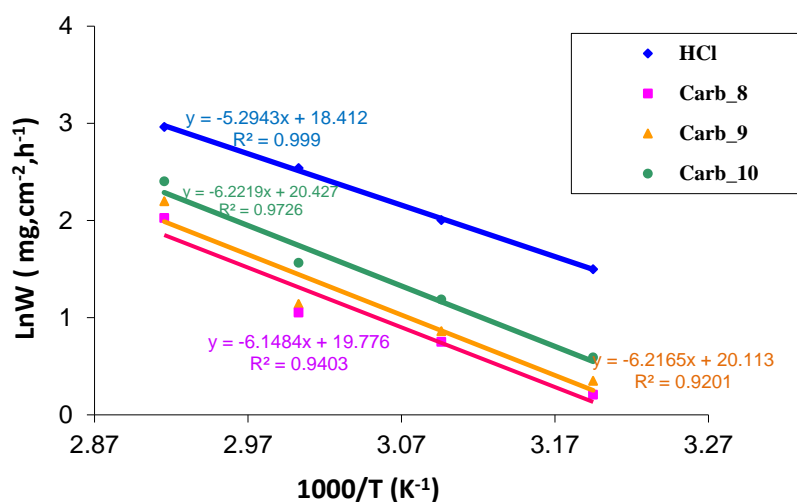
The corrosion rate of steel increases with temperature in the presence and absence of the inhibitors in the corrosive medium. It increases rapidly without the inhibitor. This result shows that the presence of inhibitors delays the corrosion rate.

3.4. Activation parameters E_a, ΔS^o_a, ΔH°_a

Different activation parameters such as the activation energy E°_a, the activated entropy ΔS°_a, and the enthalpy ΔH°_a were calculated using the Arrhenius equation (Eq. (3)) and the transition state equation (Eq. (4)) [12].

The activation energy (E°_a) was obtained from the slope ($-E^{\circ}_a/R$) of the curve of the logarithm of the corrosion rate versus the inverse of the absolute temperature. Figure 4 illustrates the variations of Ln(W) as function ($10^3/T$) without and with inhibitors.

Moreover, the enthalpy of activation ΔH°_a and the entropy of activation ΔS°_a were calculated from the plot of Ln(W/T) *vs.* 1/T graph showed in Figure 4. Straight lines are determined with a slope of ($\Delta H^{\circ}_a/R$) and an intercept of (lnR/Nh+$\Delta S^{\circ}_a/R$) from which the values of the kinetic parameters were determined and depicted in Table 4.

Figure 4. Arrhenius plots for the corrosion rate of steel in molar hydrochloric acid without and with compounds **Carb_8** and **Carb_10**

The obtained values for the activation energies from the slopes are 44.09 kJ.mol^{-1} for the uninhibited medium and 51.81, 51.77 and 51.20 kJ.mol^{-1} for the inhibited medium in the presence of 1 mol/L of **Carb_8**, **Carb_9** and **Carb_10** respectively. So, E°_a values for

inhibited systems are higher than $E°_a$ for uninhibited systems. It was found that the better inhibitor (**Carb_ 8**) shows the highest values of activation energy for the corrosion process. i.e, E_a values increase in the same order as the inhibitory efficiency [21]. In addition, the value of $E°_a$ that is around 40–80 kJ.mol^{-1} can be considered to obey the physical adsorption (physisorption) mechanism [22] which is with the results of our study.

Table 4. Corrosion kinetic parameters: $E°_a$, $\Delta H°_a$,$\Delta S°_a$ for mild steel in molar hydrochloric acid with and without of **Carb_8** and **Carb_10**

	$E°_a$	$\Delta H°a$	$E–\Delta H°a$	$\Delta S°a$
	(kJ. mol^{-1})	*(kJ.mol^{-1})*	*(kJ. mol^{-1})*	*(J. mol^{-1} .K^{-1})*
1M HCl	44.09	41.36	2.7	103.50
Carb_8	51.81	49.08	2.7	101.27
Carb_9	51.77	49.04	2.7	100.46
Carb_10	51.20	48.47	2.7	100.11

Further, the plots of Ln (W/T) versus 10^3/T (Figure 5) yielded straight lines with an intercept of (Ln(R/Nh) + ($\Delta S°_a$/R)) and a slope of (-$\Delta H°_a$/R) from which the values of $\Delta H°_a$ and $\Delta S°_a$ were determined using Eq. (4). The results are recorded in Table 4.
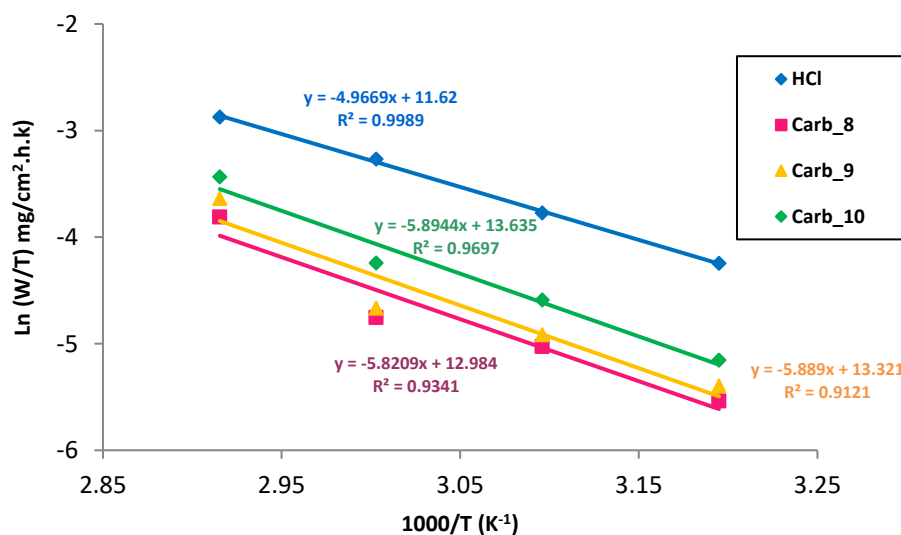
Figure 5. The corrosion (W) rates of mild steel at the transition-state in 1 M HCl in the absence and presence of compounds **Carb_8** and **Carb_10**

Furthermore, the analysis of the data in Table 4 shows that the $\Delta H°_a$ values for the dissolution reaction of mild steel in the molar chloride acid medium in the presence of 1mol/L of compounds **Carb_8** and **Carb_10** are higher than those of the uninhibited system. The

positive values of $\Delta H°_a$ indicate the endothermic nature of the mild steel dissolution process, implying that the dissolution of mild steel is retarded in the presence of inhibitors [23].

Typically, the enthalpy values below 80 kJ.mol^{-1} indicate that the adsorption process is physical while values approaching 100 kJ.mol^{-1} indicate chemisorption [24]. Contrariwise, the negative signs of the activation entropies ($\Delta S°_a$) reflect that the activated complex in the rate-determining step is an association step instead of a dissociation step, indicating that a decrease in disordering occurs on going from reactants to the activated complex [25].

Moreover, the mean value of $E°_a$-$\Delta H°_a$ is 2.7 kJ.mol^{-1}, which is about equal to the mean value of RT (2.7 kJ.mol^{-1}) at the temperature of the domain studied (333 K). This result confirms that the corrosion process is a unimolecular reaction described by the known perfect gas equation (Eq. 10) [26]:

$$E°_a − \Delta H°_a = RT \qquad (10)$$

3.5. Adsorption isotherm and energy of adsorption, ΔG_0 ads

The variation of surface coverage θ against the inhibitor concentration C shows the nature of adsorption. Adsorption isotherms are particularly important to understanding the mechanism of inhibition-corrosion reactions. Langmuir adsorption isotherms are the most commonly used [27], Temkin [28], and Frumkin [29]. In this study, the surface coverage θ values were determined graphically to search for an appropriate adsorption isotherm. Plotting the curve versus C yields a straight line (Figure 6), which proves that the adsorption of inhibitors on the steel surface fits the Freundlich adsorption isotherm ($\theta = K_{ads} C$).

The standard adsorption free energy (ΔG_{ads}) is calculated through the equation below (Eq. 11) [30]:

$$K = 1/55,5 \exp(-\Delta G_{ads}/RT) \qquad (11)$$

where K is the adsorption reaction's equilibrium constant.

The resulting values of ΔG_{ads} are:

- $\Delta G°_{ads}$= -12.42kJ/mol for **Carb_ 8** ;
- $\Delta G°_{ads}$= -12.12 kJ/mol for **Carb_ 9** ;
- $\Delta G°_{ads}$= -12.20 kJ/mol for **Carb_10**.

The negatives ΔG_{ads} values show that the three chemical substances are spontaneously adsorbed on the metal surface [31]. Values of ΔG_{ads}>-40 kJ.mol^{-1} are interpreted by physical adsorption. Values of ΔG_{ads}<-40 KJ/mol are viewed as chemisorption fact [32]. The values of ΔG_{ads} obtained suggest that inhibitors act through physical adsorption.
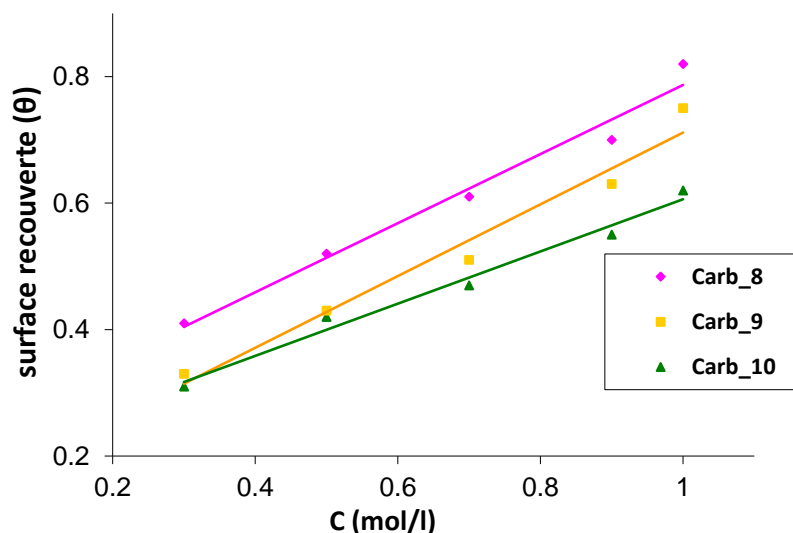
Figure 6. Variation of surface coverage θ versus the inhibitor concentration

3.6. Theoretical studies

### 3.6.1. DFT calculations

The methodologies of quantum mechanics and Monte Carlo may be essential due to the degree of complex associated with understanding a process of corrosion and inhibition via organic compounds. The structure and chemical responsiveness of molecules can be explained and predicted using molecular modeling and the evolving quantum approach [33, 34].

In that view, the Density Functional Theory study was conducted linking the inhibitive effect of the three inhibitors and their electronic properties. Figure 7 shows the optimized structures, as well as the LUMO-HOMO-EPS plots of **Carb_8**, **Carb_9**, and **Carb_10**, and Table 5 lists the descriptors that were employed in corrosion investigations as a result of DFT calculations.
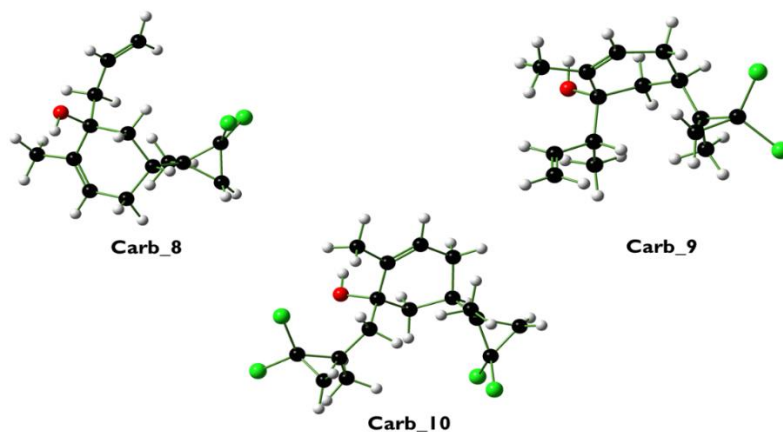
Figure 7. The optimized structures of the three inhibitors as computed by DFT on the basis set (B3LYP/6-31++G (d, p))
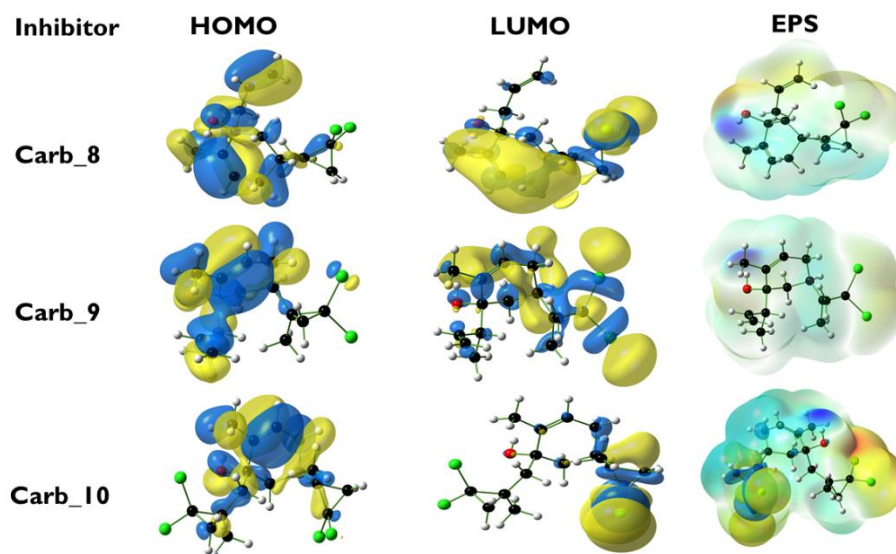
Figure 8. The HOMO-LUMO and EPS iso-surfaces for **Carb_8**, **Carb_9**, and **Carb_10**, as generated using DFT on the basis set (B3LYP/6-31++G (d, p))

As seen in Figure 8, the electron density of the HOMO is dispersed over the third inhibitors' single double bond and hydroxyl O atoms. These sorts of molecular visualizations argue that electrons, including solitary electrons, are likely to be transferred to metal locations that are lacking in electrons, resulting in donor-acceptor interactions [35]. Moreover, 1,1-dichlorocyclopropane seems to be the most appropriate atomic region for LUMO. As a result, the electron reception behavior of the metal likely occurs through its circular cyclopropylopropane atoms. These electrons can be delivered by filled orbitals of the iron atoms. The negative areas (red color) in the ESP maps, which are made up of oxygen atoms in the hydroxyl groups of the analyzed compounds, present favorable interaction sites for an electrophilic attack. The double bonds (C=C) had a small electron-rich area (yellowish white). The most positive areas (blue) on the other hand, occupy the rest of the molecule and are found over the chlorine atoms. It is known that high EHOMO values indicate the propensity of a molecule to readily give electrons to empty metallic orbitals, while the low ELUMO values show the propensity of a molecule to accept electrons from the metal [36,37]. Lower Gap energy (ΔE) values suggest a more reactive chemical.

Carb_8 has the highest E$_{HOMO}$ relative to **Carb_9** and **Carb_10**, demonstrating that both carbides have a potent chance to relate with the metal surface by providing electrons (Table 5). The expected outcomes also include low hardness and electronegativity values, which indicate the ability of the **Carb_8** inhibitor to adsorb to the iron surface. The transferred electron fraction (ΔN) of **Carb_8** [N (**Carb_8**) = 0.19] confirms its significant ability as an electron donation entity on the iron surface. The inhibitory efficacy of the **Carb_8** molecule is

confirmed because of its high dipole moment compared to that of the water molecule (1.85 D) [38]. This certainly indicates more powerful dipole-dipole interactions between the compounds that are inhibiting and the surfaces of the mild steel. Based on the data mentioned above, the inhibitory efficiency of the chemicals in question is as follows: **Carb_8** > **Carb_9** > **Carb_10**.

Table 5. Quantum chemical parameters of the compounds based on (6-31G++(d,p) basis set

| Adsorbate	E_{HOMO} (eV)	E_{LUMO} (eV)	η	χ	Dipole moment	ΔE_{Gap} (eV)	ΔN
Carb_8	-6.80	-0.54	3.13	3.67	3.76	6.26	0.19
Carb_9	-7.07	-0.67	3.20	3.87	1.86	6.41	0.15
Carb_10	-7.13	-0.70	3,21	3.92	4.3	6,43	0.17

3.6.2. Monte Carlo Simulation (MC)

To understand how the selected inhibitors interact with Fe (110) surface MC, simulations were performed. Side views of the most stable **Carb_8**, **Carb_9** and **Carb_10** adsorption configurations on the Fe surface (110) are shown in Figure 9. As well, the results descriptors computed using the MC simulation are presented in Table 6.

Table 6. Energies calculated by the Monte Carlo Simulation (in kcal/mol)

Molecule	E_{Tot}	E_{Ads}	dE_{ads}/dNi
Carb_8	**-5 733.57**	**-5 925.29**	**-85.79**
Carb_9	**-5 539.77**	**-5 642.11**	**-91.67**
Carb_10	**-5 057.96**	**-5 150.34**	**-86.33**

All three inhibitor molecules are adsorbed by their chlorine and oxygen atoms (**Carb_9** and **Carb_10**), or via the double bond in the case of **Carb_8** (Figure 9). **Carb_8** has larger negative adsorption energy, as shown in Table 6. This trend is supported by most quantum chemistry simulations and experimental evidence.

The adsorption energies (E_{Ads}) of the selected inhibitors are negative, which means that the adsorption process is spontaneous and stable, requiring an exo-thermal reaction [39].
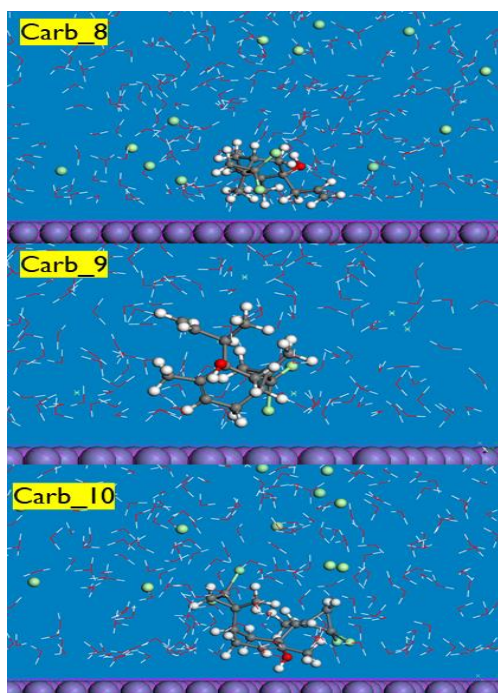
Figure 9. side view of the stable adsorption configurations for the adsorption of the examined compounds on Fe (110)

4. CONCLUSION

To sum up, the main conclusions of this work can be summarized as follows:

- The dichlorocyclopropanation reaction is regioselective for allylcarveols **5** and **6**, but not for **7**;
- It was found that corrosion of carbon steel in acid was significantly delayed in the presence of **Carb_8**, **Carb_9** and **Carb_10**;
- Synthesized compounds effectively prevent corrosion of steel in an HCl environment;
- The inhibition efficiency increases by increasing concentration;
- Freundlich's isothermal adsorption model regulates the adsorption of synthesized molecules to the surface of the steel in molar hydrochloric acid;
- The theoretical results demonstrated good consistency with the results of the weight loss measurements.

REFERENCES

[1] F. Bentiss, M. Traisnel, and M. Lagrenée, Corros. Sci. 42 (2000) 127.

[2] M. El Azhar, B. Mernari, M. Traisnel, F. Bentiss, and M. Lagrenée, Corros. Sci. 43 (2001) 2229.

[3] X.L. Cheng, H.Y., Ma, S.H. Chen, R. Yu, X. Chen, and Z.M. Yao, Corros. Sci. 41 (1999) 321.

[4]   A. Bouyanzer, B. Hammouti, and L. Majidi, Mater. Lett. 60 (2006) 2840.

[5]   B. Zerga, M. Sfaira, Z. Rais, M. Ebn Touhami, M. Taleb, B. Hammouti, B. Imelouane, and A. Elbachiri, Mater. Technol. 97 (2009) 297.

[6]   M. Znini, L. Majidi, A. Bouyanzer, J. Paolini, J-M. Desjobert, J. Costa, and B. Hammouti, J. Arab. Chem. (2010). doi: 10.1016/j.arabjc.2010.09.017

[7]   Z. Faska, , L. Majidi, R. Fihi, A. Bouyanzer, and B. Hamouti, Pigm. Resin Technol. 36 (2007) 293.

[8]   Z. Faska, A. Bellioua, M. Bouklah, L. Majidi, R. Fihi, A. Bouyanzer, and B. Hammouti, Monatsh. Chem. 139 (2008) 1417.

[9]   L. Majidi, Z. Faska, M. Znini, S. Kharchouf, A. Bouyanzer, and B. Hammouti, J. Mater.Environ. Sci. 1 (2010) 219.

[10]   S. Kharchouf, L. Majidi, M. Znini, J. Costa, B. Hammouti, and J. Paolini, Int. J. Electrochem. Sci. 7 (2012) 10.

[11]   F. Bentiss, M. Lebrini, H. Vezin, F. Chai, M. Traisnel, and M. Lagrene, Corr. Sci. 51 (2005) 2165.

[12]   L. Messaadia, O.ID El mouden, A. Anejjar, M. Messali, R. Salghi, O.Benali, O.Cherkaoui, and A. Lallam, J. Mater. Environ. Sci. 6 (2015) 598.

[13]   R.I. Masel, Principles of Adsorption and Reaction on Solid Surfaces. Willey, New York (1996).

[14]   B. Ngouné, M. Pengou, A. M. Nouteza, C. P. Nanseu-Njiki, and E. Ngameni, ACS Omega 4 (2019) 9081.

[15]   M. Damej, R. Hsissou, A. Berisha, K. Azgaou, M. Sadiku, M. Benmessaoud, N. Labjar, and S. El hajjaji, J. Mol. Struct. 1254 (2022) 132425.

[16]   M. Oubaaqa, M. Rbaa, M. Ouakki, R. Idouhli, M. Maatallah, A. Jarid, and M. Ebn Touhami, J. Appl. Electrochem. 52 (2022) 413.

[17]   M. Murmu, SK. Saha, NC. Murmu, and P. Banerjee, Corros. Sci 146 (2019) 134.

[18]   Materials Studio Revision 8.0 (2016) Accelrys Software Inc.: San Diego, CA, USA

[19]   S. Kharchouf, L. Majidi, M. Bouklah, B. Hammouti, A. Bouyanzer, and A. Aouniti, J. Appl. Electrochem. 7 (2014) 680.

[20]   C. Fiaud, A. Harch, D. Mallouh, and M. Tzinmann, Corros. Sci. 35 (1993) 1437.

[21]   R. Gasparac, and E. Stupnisek-Lisac, Corrosion 55 (1999)1031.

[22]   K.O. Orubite, and N.C. Oforka, Mater. Lett. 58 (2004) 1772.

[23]   N.M. Guan, L. Xueming, L. Fei, Mater. Chem. Phys. 86 (2004) 59.

[24]   S. Martinez, and I.Stern, Appl. Surf. Sci. 199 (2002) 83.

[25]   S. Samkarapapaavinasam and M.F. Ahmed, J. Appl. Electrochem. 22 (1992) 390.

[26]   F. Bentiss, M. Lebrini, M. Lagrenée, M. Traisnel, A. Elfarouk, and H. Vezin, Electrochim. Acta 52 (2007) 6865.

[27]   I. Langmuir, J. Am. Chem. Soc. 39 (1947) 1848.

[28] A.N.Z. Frumkin, Phys. Chem. 116 (1925) 466.

[29] J.H. de Boer, The Dynamical Character of Adsorption, seconded. Claredon Press, Oxford, UK (1968).

[30] E. Khamis, Corrosion. 46 (1990) 476.

[31] Z. Szlarska-Smialowska, Corros. Sci. 18 (1978) 557.

[32] G.M. Barrow, Phisical chemistry. 4th ed. New York: McGraw-Hill (1983) pp. 739.

[33] R. Oukhrib, Y. Abdellaoui, A. Berisha, H. Abou Oualid, J. Halili, K. Jusufi, and C. Len, Sci. Rep. 11 (2021) 1.

[34] I. B. Obot, S. Kaya, C. Kaya, and B. Tüzün, Phys. E: Low-Dimens. Syst. Nanostructures, 80 (2016) 82.

[35] A. Abdeslam, L. Zouhair, M. Znini, M. Mounir, and L. Amal, Anal. Bioanal. Chem. 8 (2021) 113.

[36] A. Abdeslam, M. Mounir, Z. Mohamed, L. Zouhair, and A. Mohamed, Mediterr. J. Chem. 10 (2020) 62.

[37] A. Regti, Z. Lakbaibi, H. Ben El Ayouchia, M. El Haddad, M. R. Laamari, M. El Himri, and R. Haounati, Int. J. Environ. Anal. Chem. 1 (2021) 20.

[38] A. El Asri, A. Jmiai, M. M. Rguiti, R. Oukhrib, K. Abbiche, H. Zejli, and S. El Issami, J. Mol. Liq. 345 (2022) 117813.

[39] TA. Salman, DS. Zinad, SH. Jaber, M. Al-Ghezi, A. Mahal, MS. Takriff, and AA. Al-Amiery, J. Bio. Tribo. Corros. 5 (2019) 1.